CEAS Aeronautical Journal (2023) 14:139–154
https://doi.org/10.1007/s13272-022-00624-z

ORIGINAL PAPER

Aerodynamic validation for compressor blades' structural morphing concepts

Zhuzhell Montano Rejas[1,3] · Marcel Seidler[2,3] · Johannes Riemenschneider[1,3] · Jens Friedrichs[2,3]

Received: 28 February 2022 / Revised: 9 September 2022 / Accepted: 19 October 2022 / Published online: 24 November 2022

Abstract

For increasing an aircraft's engine efficiency and reducing emissions, the use of adaptive blades capable of guaranteeing an optimal performance at different flight phases is researched. An aerodynamic design point blade shape and some exemplary possible morphed shapes for different operational conditions are introduced and analyzed from a structural as well as from an aerodynamic point of view. For this purpose, the structural design process developed to calculate the blade geometries that can be reached through structurally integrated actuation is introduced and explained with the help of three morphing blade example geometries. Furthermore, the aerodynamic methods used for the evaluation of the structurally achieved morphed geometries is also studied with the help of the introduced examples.

Keywords Morphing compressor blades · Aerostructural coupled design

Abbreviations

ACP	ANSYS composite PrepPost
AVDR	Axial velocity density ratio
CAD	Computer aided design
CFD	Computational fluid dynamics
CFRP	Carbon fiber reinforced plastics
CMC	Ceramic matrix composites
corr.	Corrected
DP	Design point
FEA	Finite element analysis
IGV	Inlet guide vane
LE	Leading edge
MF	Mass flow
MFC	Macrofiber composite
MPC	Multipoint constraint
OGV	Outlet guide vane
PM	Performance map
PR	Pressure ratio
PS	Pressure side
SA	Shape adaption
SLC	Streamline curvature
SMA	Shape memory alloy
SS	Suction side

Symbols

R	Radius
X,Y	2D coordinates
$\Delta\beta 1$	Relative inflow angle variation
$\Delta\kappa 1$	Leading edge metal angle variation
$\Delta\Delta\varphi$	Profile turning morphing
ω	Pressure loss coefficient
$\dot{m}$	Mass flow

1 Introduction and motivation

To reduce an aircraft's polluting emissions and to comply with international environmental goals for a sustainable and eco-friendly aviation, it is necessary to re-design current engine designs, focusing on a high performance during all flight phases and becoming adaptable. Since the engine's performance and therefore the compressor performance is crucial for an aircraft's overall efficiency, one can increase performance by designing compressor blades capable of adapting themselves to different flying conditions [1, 2].

✉ Zhuzhell Montano Rejas
Zhuzhell.MontanoRejas@dlr.de

[1] German Aerospace Center (DLR), Institute of Composite Structures and Adaptive Systems, Lilienthalplatz 7, Brunswick, Germany

[2] Institute of Jet Propulsion and Turbomachinery, Technische Universität Braunschweig, Hermann-Blenk-Strasse 37, Brunswick, Germany

[3] Sustainable and Energy Efficient Aviation (SE2A), Brunswick, Germany

Currently available compressor blades are commonly made of titanium alloys or superalloys and are designed and manufactured with a monolithic architecture. With the introduction of carbon fiber-reinforced plastics (CFRP) for larger blades, such as those in the fan, and of ceramic matrix composites (CMCs) in blades of the first turbine stages, the potential of composite blade structures for achieving a better performance while reducing weight has been shown [3–6]. Shape adaptive systems have, however, not yet been included in such architectures, and currently available flow control measures for bladed components consist of systems such as inlet guide vanes (IGVs) or outlet guide vanes (OGVs). These systems can regulate the mass flow by turning along hinged mechanisms and, as a result, change the incidence angle of the blades. Because of the hinged mechanisms, they are still limited to constant spanwise pitch angle variations [7, 8]. Other proposed mechanisms aim to overcome the rigid shape movement of IGV like systems by adding rigid flaps and variable tandem blades to them [9]. In this way, they are capable of adding a turning variability and achieving an increased operational range. An application of blade pitch control within a rotating system has been reported in [11], where the off-design operation of a highly loaded fan stage was improved by adapting the fan pitch according to the flow incidence under part-load, off-design conditions. The benefits of pitch variable fan blading in terms of thrust maximization and specific fuel consumption under take-off conditions for short take-off and landing (STOL) transport aircraft concepts have been emphasized by Ref. [12]. An alternative to mechanical incidence adaption measures has been proposed by Ref. [13], who numerically and experimentally investigated aspiration and fluid injection at the domain end walls. By including active flow control mechanisms in the first stator row, corner separation in part-load operation could be suppressed, which improved overall compressor efficiency.

Such mechanisms are, however, quite complex, depending on additional components for functioning. Because of this, weight is added to the engine and the need for maintenance and repair is increased. Despite allowing for a radially constant adaption, systems with variable stator or rotor pitch lack flexibility and therefore no local blade modifications are feasible.

Within the frame of the Sustainable and Energy Efficient Aviation Excellence Cluster (SE^2A), the use of structurally integrated actuators for current, complex, highly 3D (regarding spanwise twist, camber and thickness variations) compressor blade shapes are investigated. By structurally morphing the blade shapes, an improvement of the blade, stage and overall engine efficiency is expected under off-design operational conditions. Depending on pre-defined operational off-design scenarios, either the spanwise blade twist, turning or both parameters are targeted for the shape morphing [14]. Through a tailored, composite architecture for the actuators and through their integration in the blade's body, the adaptability of the blade is increased and targeted shape variations in spanwise direction can be achieved. As a result, the blade shape is specifically adapted for the selected off-design flow conditions. The overall goal of the morphing blade concept is to increase aerodynamic performance by structurally morphing the blade's structure, without increasing mechanical system complexity, while maintaining or even reducing weight.

For this purpose, a design methodology has been introduced, which couples the aerodynamic and structural aspects for the design of shape adaptive compressor blading [14]. The design process is split into three steps and depends on different aerodynamic evaluation approaches, which have to comply with the respective requirements in terms of evaluation fidelity and rapidity. In literature, coupling approaches of varying complexity are described. [15] combined with an analytical structural model based on the Euler–Bernoulli–Beam theory with a potential flow solver to evaluate the impact of a morphing airfoil camber for fixed-wing aircraft or helicopter blading. For the numerical evaluation of morphing wind turbine blading, Ref. [16] used surface pressure distributions and mesh displacements for a two-way coupling within the ANSYS Workbench. An overview of further coupling approaches, their numerical requirements and their respective challenges is given in Ref. [17], where complex meshes and calculation domains as a hitch for moving mesh techniques are especially emphasized.

Within this research, the aerostructural coupling is integrated in a pre-design methodology, which is based on a re-engineering approach for deteriorated rotor blading [18]. While the coupling approach is described in Refs. [14, 19], this research focusses on the aerodynamic assessment methodologies of the shape morphing potential. Starting with the transformation of the feasible deformations into aerodynamic blade design angles, a near 3D or Q3D simulation approach is introduced to include viscous effects and blade-shock interactions. A three-dimensional stage simulation approach of the morphed rotor geometry describes the last evaluation step with the highest accuracy, but also the highest computational requirements.

For the study of aerodynamic sensitivities within the evaluation approaches, three different actuation concepts are researched. For the structural analysis finite element analysis (FEA) simulations allowing to calculate the morphed shapes are performed.

2 Morphing blades functioning principle

The here considered morphing blades are composite blade structures consisting of a main blade body onto which surface actuators have been structurally integrated. As in

conventional blades, the blade's body can be made of traditional materials, such as titanium alloys, or of alternative materials, such as composites. The actuators can be made of any active materials capable of modifying the main body's structure. When active, the actuators can expand or contract, changing their shape. The forces generated through these changes are transferred to the blade's main body, leading to a shape modification of the whole blade. An exemplary architecture of such a blade structure is shown in Fig. 1.

The considered actuators for morphing compressor blades applications are piezoelectric macrofiber-composite (MFC) actuators and SMA actuators. These actuators can be made of thin piezoelectric material fibers or SMA fibers or thin SMA foils, respectively. The active fibers or foils are integrated into a flexible material support to build the actuator and to enable the structural force transmission [20, 21]. The exemplary study presented here focuses on MFC actuators, SMAs will therefore not be further discussed in the presented analysis. A schematic representation of an MFC actuator is illustrated in Fig. 2.

When exposed to an electric field, the fibers expand or contract and change the shape of the actuator. Once integrated into a structure, these deformations produce loads that are directly transferred from the actuator into the surrounding blade's body, deforming it and leading to shape adaption. Since the fibers expand and contract lengthwise, the overall deformation follows the fiber direction. It is this directional change what allows for a targeted shape control and what enables their specific application for morphing compressor blades.

By using different actuators on the pressure and suction sides of the blade and by assigning different actuating directions to each, it is possible to reach a wide variety of

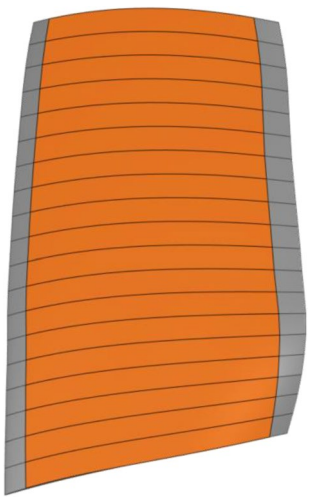

Fig. 1 Exemplary blade body (gray) with integrated surface actuator (orange)

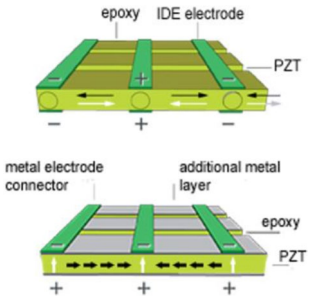

Fig. 2 Piezo actuators working principle [20]

morphing shapes. By expanding or contracting, the integrated actuators are capable of achieving the desired aerodynamic shapes for off-design operating conditions in a targeted manner. Targeted modifications of characteristic blade angles such as the spanwise turning and stagger angles are therefore possible.

3 Aerostructural design coupling methodology

The aerostructural design coupling methodology starts with an initial, reference compressor design. At the same time, different off-design requirements for the compressor and for common aircraft missions are considered. A streamline curvature calculation for the selected off-design scenario yields the desirable variations in spanwise flow angles [14]. Depending on the dominant morphing requirements, a morphing target for the structural deformation simulations is then selected. The blade reference shape and the inflow and flow turning requirements are set for pre-defined meridional streamlines through the blading. These stream sections are kept constant within the design process and serve therefore as an input for the structural design process [19].

Having received these geometric boundary conditions and considering environmental and operational boundary conditions, such as working environment temperatures, the structural design process begins with the morphing blade model development. With the help of the reference blade, a geometric design for a blade with integrated actuators is developed. A set of parameters covering the geometry of the blade and that of the actuators, the actuation direction and the material possibilities, both for the blade and for the actuators are considered for this design. Based on all the inputs and parameters, different possible morphing shapes can be determined. The results on achievable morphing shapes for the aerodynamic sections of the reference design are then calculated and given back to the aerodynamics for verification and validation. This closes the loop of the design process, coupling both disciplines. The whole is an iterative

process that is run until a shape that respects both aerodynamic and structural boundary conditions for an improved performance has been achieved.

The coupled analysis itself happens in three stages:

1) Based on the compressor reference design and on the off-design conditions, a qualitative comparison of aerodynamically desirable and structurally achievable blade profile angle variations, such as blade staggering and profile turning is conducted. This starting analysis is based on the evaluation of the morphed blade shape according to aerodynamic design criteria.
2) In a second step, a representative Q3D-CFD simulation is conducted for a tip section of the deformed rotor to include effects such as viscous losses or blade–shock interactions in the analysis.
3) In the final stage of the coupled design detailed three-dimensional simulations, both for the structure and for the aerodynamics are performed. This allows to get detailed results for the morphing blade's behavior under design and off-design conditions.

4 Test case: NASA67 rotor

For this research, the well-studied NASA67 front stage rotor was chosen [22, 23]. This rotor has been widely researched and tested and extensive design data, including the geometry, is accessible. Furthermore, this rotor is transonic in the blade tip region, which is beneficial for shape adaption, since under this aerodynamic regime even small shape changes in blade geometry can lead to considerable effects in the aerodynamic behavior of the whole blade.

Next to the blade reference geometry, the design methodology requires the operating behavior of the stage. To obtain its performance map, consisting of the achievable pressure ratios and isentropic efficiencies depending on the mass flows through the stage, stationary 3D-RANS simulations are conducted for design rotational speed. The calculation domain consists of one rotor and stator row, with a mixing plane interface between the rotating and stationary domains. Fillets are considered for both the stator and the rotor. With a total pressure and temperature at the inlet, the speed lines are derived by gradually increasing the static back pressure behind the stator, until numerical instabilities predict the numerical surge limit. To minimize the iteration error within the CFD simulations, a constant mass flow and isentropic efficiency were defined as convergence criteria, while the target for the mean momentum, continuity and total energy residuals was set to a maximum of 10^{-4}. A structured mesh with $y^+ \approx 1$ at the hub, shroud and at the blades' surface is created with the meshing software Numeca AutoGrid5 to fully resolve the near wall flows, especially in the transonic regimes of the chosen test case. To avoid any mesh dependency of the results, a grid convergence study is conducted with special emphasis on the isentropic Mach number distribution at 95% blade height and an asymptotic mesh convergence behavior, according to the grid convergence index (GCI). With a GCI below 0.01% for the design point pressure ratio, mass flow and isentropic efficiency, the chosen mesh resolution achieved the expected grid convergence behavior. Different turbulence models were simulated, yielding the speed lines displayed in Fig. 3. For the setup, the k–ω turbulence model was chosen as a compromise between simulation time costs and accuracy.

Based on the selected numerical CFD setup, a reference speed line can be defined, which allows to derive shape morphing scenarios. The resulting performance map (PM line) is displayed in Fig. 4 with the literature design point (DP) of the stage (shown in red) and three possible shape adaption (SA) scenarios:

1) An extension of the surge margin (green, SA: PM), where the operational range is enlarged for an increased surge margin and efficiency also under lower mass flow conditions.
2) An adjustment of the pressure ratio (yellow, SA: PR), for an elevated pressure ratio under equal mass flow conditions.
3) An adjustment of the mass flow (blue, SA: MF), for being able to operate at higher mass flows without losses in pressure ratio.

Those scenarios then define the second basis for the aerostructural design methodology. Based on these, idealized aerodynamic deformation requirements are derived, which then serve as an optimization target for the application of

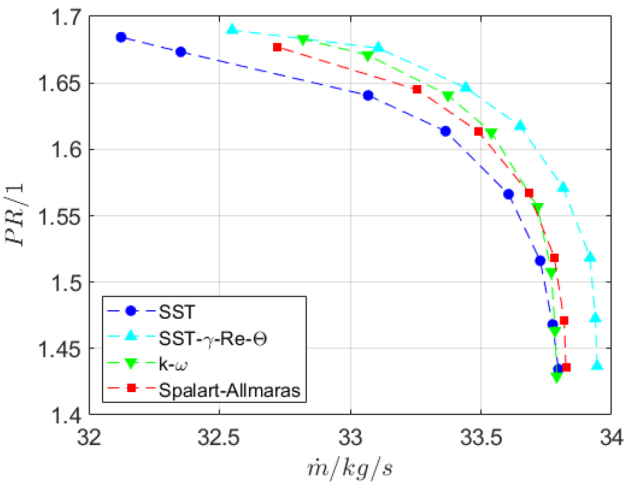

Fig. 3 Performance maps of the NASA67 rotor with different turbulence models

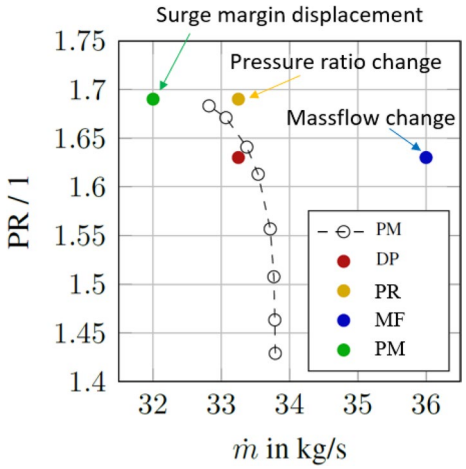

Fig. 4 NASA67 rotor performance map and morphing scenarios, with PR the pressure ratio and ṁ the mass flow

surface actuators to the pressure and suction sides of the reference blade. With the goal to modify the actuated blade shape according to the pre-defined deformation targets flow incidence and deviation for the selected off-design scenario are reduced.

5 Structural analysis

The structural analysis takes as a basis the aerodynamic sections that result from the meridional design of the blade. These profile sections represent the direction of the airflow through the blade, which allows to maintain aerodynamic characteristics throughout the structural simulation. Current blade design approaches used by the industry such as the one in Ref. [24] preserve the aerodynamic sections for rigid blade architectures design. This facilitates a coupled analysis between aerodynamics and structure. In order to follow this guideline and to facilitate the introduction of morphing blade technologies to industrial applications and future engines and aircraft, the reference meridional sections are also kept throughout the morphing blade's structural analysis and development method. In addition to facilitating the multidisciplinary coupling, this also adds flexibility to the structural design process, since the method can be applied to any reference meridional design blade geometry. This also includes currently common highly complex 3D blade architectures with different camber and twist angles along the blade, as well as with a strong thickness variability. Furthermore, all this is possible while using common engineering tools and allowing for a rapid calculation of possible actuator configurations.

The first step in the structural design process is to calculate and parametrize the geometry of the morphing blade

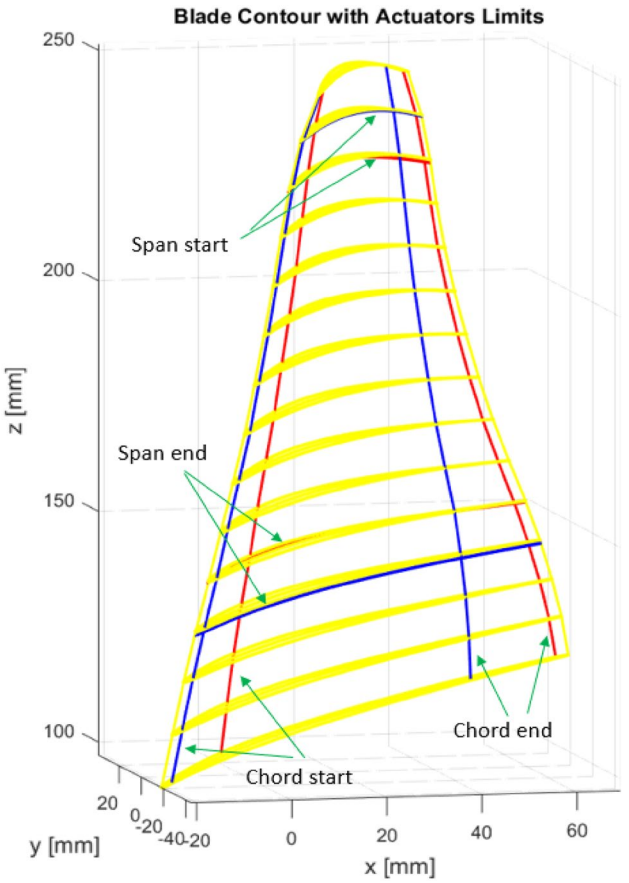

Fig. 5 Parametric geometry of the blade. Yellow lines: meridional geometry of the blade. Blue and red lines: geometric limits of the actuators

based on the reference aerodynamic blade sections. The studied design variables are values describing the geometry of the actuators and their actuation behavior. For implementing this, a program developed with Matlab creates sets of possible geometric parameters for the actuators. These parameters allow controlling the actuators' sizes and positions on the blade based on their thicknesses and on their relative spanwise and chordwise starting and ending positions. In addition, the desired actuation directions and modes can also be controlled (Fig. 5 and Table 1). The parameters cover both the pressure as well as the suction sides of the blade. Since larger surface actuators lead to larger deformations, the developed model focuses on the use of two large surface actuators, one for the pressure side and one for the suction side. By varying the relative positions of the actuators toward one another and by varying the actuation directions and modes of each one of them, it is possible to achieve the targeted modifications of the blade's shape. Possible target deformations can for example aim for a maximization of the metal or the turning

Table 1 Actuators geometric parameters for models (for pressure side (PS) and suction side (SS) actuators, respectively, with start < end; comp.: compression, exp.: expansion)

Parameter	Range	Reference
Chord start PS	5–95%	Chord length
Chord end PS	5–95%	Chord length
Span start PS[a]	0–100%	Span length
Span end PS[a]	0–100%	Span length
Actuation direction PS	0–180°	Rosettes as in Sect. 5.1
Chord start SS	5–95%	Chord length
Chord end SS	5–95%	Chord length
Span start SS[a]	0–100%	Span length
Span end SS[a]	0–100%	Span length
Actuation direction SS	0–180°	Rosettes as in Sect. 5.1
Actuation mode[a]	comp./exp./off	Boundary conditions

[a]Not used in this study

angles or for modifications of the stagger angle or the position of the maximum camber of the blade.

This geometric set of parameters and the common profile sections are used as a basis to create the structural models, first as CAD designs and later on as FEA models. For this, the Matlab modeling process sends the optimized geometric parameters related to the blade and to the actuators to ANSYS SpaceClaim to automatically generate CAD models for the components. These models are then loaded onto an ANSYS Workbench project. There, the structural analysis is carried out with the help of a project block structure following the approach shown in Fig. 6.

The first block contains all the material information for the blades and for the actuators. Using this block, it is possible to assign different materials, and therefore properties, to all elements, making it possible to test different morphing shape possibilities such as more twist or camber for the blade based on material properties. The blade material that was considered for this analysis is a titanium alloy (Table 2), homogeneously distributed throughout the blade's body. This material was chosen because it is currently the most common for compressor blade applications.

The second block builds up the mechanical models for the basis blade without actuators and, separately, for the actuators. The blade is represented as a solid body and meshed accordingly. A regular mesh with quadratic elements and fine enough to offer transferable results for the aerodynamics was chosen. The actuators are represented and meshed as shell elements, because their thickness (0.3–0.6 mm) is considerably smaller than their width (ca. 9 cm) and length (ca. 16 cm). The use of shell elements for this application reduces time simulation costs that would be higher for the otherwise necessary very fine solid mesh. Furthermore, it does not reduce accuracy, with a variation of only 0.2–2% in

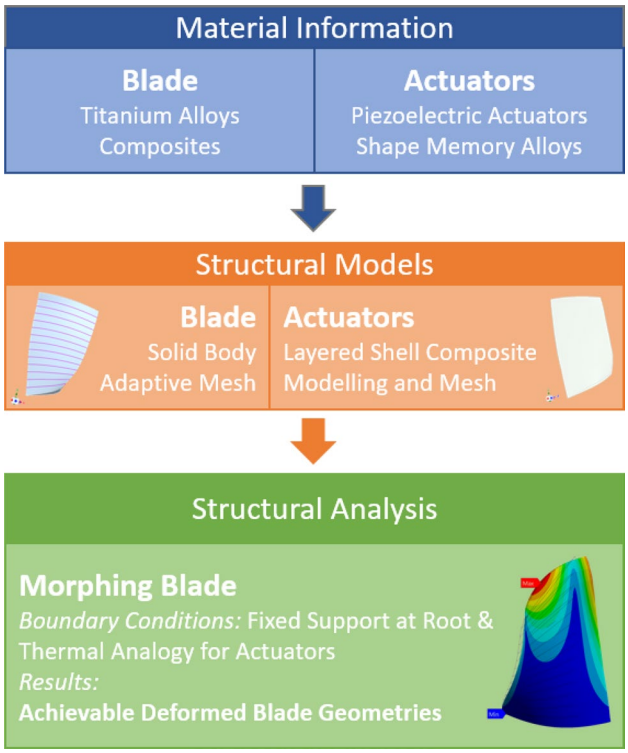

Fig. 6 Structural design process

deformation results compared to solid element models. The material properties of the actuators are controlled through the Ansys Composite Pre–Post (ACP) tool. This tool enables the modeling of the actuators as fiber composite materials, controlling the number of actuation layers or stack-ups, as well as the actuation direction through the fibers' directions.

All models are brought together in the structural analysis block, where a static structural analysis for the morphing blade as one body is carried out. Here, the contacts between the blade and the actuators are modeled as bonded contacts with the help of the ANSYS multipoint constraint (MPC) approach, so that the transmission of force from the actuators is directly conveyed toward the blade and can, as a result, lead toward the desired morphing shapes. For such a contact modeling approach, no alignment between the solid and shell meshes is necessary. The contact surfaces are given

Table 2 Titanium alloy properties for basis blade model

Property	Value	Unit
Density	4620	kg/m^3
Young's modulus	9,6E10	Pa
Poisson's ratio	0,36	–
Shear modulus	3,5294E10	Pa
Tensile yield strength	9,3E8	Pa

by the actuator shell elements and the target surfaces by the blade's solid elements.

In addition to the contact boundary conditions, the actuator behavior as such is modeled with the help of a thermal analogy boundary condition, allowing to describe the expansion or contraction behavior of the shell elements due to the presence of an electric field for piezo actuators or to temperature changes for shape memory alloys (SMAs). This analogy offers the introduction of strains in a very simplified approach without the need for major changes to the modeling process and allows obtaining a reference model for the morphing behavior of the blade, which can be further tuned in a detailed design. To do this simplification, coefficient of thermal expansion values recreate the actuators expansion or contraction behavior. These coefficients, together with the corresponding temperature boundary conditions, simulate the actuation process. The values are calculated based on the strain and electric field or thermal expansion properties of the respective actuating material. For example, to simulate the electric deformation behavior under a given voltage for a piezoelectric actuator, the thermal coefficient allows obtaining the same deformation value, only under thermal boundary conditions instead of electric ones. The mechanical properties of the actuators in the thermal analogy are also exactly the same, and no thermal dilation behavior is considered for the blade, so that only the mechanical actuation effects are transferred from the actuators into the blade's structure, as is the case when using structurally integrated actuators. Effects such as actuation non-linearities and hysteresis are not accounted for in this much simplified model.

The root of the blade is modeled as a fully fixed surface in a simplified representation. Based on this, the possible deformations that can be achieved through the chosen actuators are calculated at the aerodynamic sections originally set by the streamlines and exported back as input for the aerodynamic analysis.

5.1 Actuation modeling

To model the actuation behavior, the ACP module of ANSYS is used, since it allows to easily assign different materials to the actuators, to create stack-ups and to modify the fiber, and therefore the actuation, directions (Fig. 7).

Having large actuating surfaces and therefore a larger amount of piezo-actuating fibers, it is possible to reach larger deformations, since more actuating material and a longer lever arm for the actuation force are directly available. By using more than two surface actuators (one on the pressure side and one on the suction side), it is possible to create a wider range of morphing shape variations. However, with more but smaller actuators and the required spaces between them, the amount of actuating fibers and the effective actuating surfaces decrease, diminishing the reachable morphing

Fig. 7 ACP actuator model with actuation directions for the pressure side shown in green

amplitudes. To be able to minimize the number of actuators and at the same time enlarge the morphing possibilities for the blade, an optimization approach capable of designing a blade with a targeted tuning of the actuating directions for specific aerodynamic and structural shapes is necessary. With currently available MFC actuators, the possible deformations remain small, reaching up to ~ 0.8 mm for a twist deformation at the tip, for the NASA67 blade with two large surface actuators (blade dimensions: ~ 95 mm chord length and ~ 150 mm span). To maximize morphing, and therefore also reach the strongest possible influence on the aerodynamics, the use of two large surface actuators covering the whole blade span has been shown to be the most promising configuration. For this, three possible blade morphing possibilities have been considered: twist, camber maximization and a displacement of the maximum camber.

The parameters at play to reach such morphing blade target shapes are the actuators' thicknesses (defined by how many actuators are in a stack-up configuration), the actuating direction and whether they are set for expansion or compression. For a simplified approach, the same actuation capabilities are assumed for expansion as well as for compression. For a detailed analysis, these values have to be however modified, since MFC actuators can expand more than they can contract.

5.2 Morphing shapes

Through the parameter variations introduced in Sect. 5.1, it is possible to achieve a wide variety of changes in parameters describing the blade, such as the maximum camber, the position of the maximum camber or the stagger angle. Depending on the aerodynamic goals, different possibilities

can lead to beneficial aerodynamic effects. Figures 8, 9, and 10 show three examples of such possible morphing shapes. In the illustrations the contour of the reference geometry is displayed in black, while the total deformations at the meridional sections are displayed in color. In Fig. 8, the morphing shape for an actuation configuration aiming to maximize the metal angle of the blade is presented. As it can be seen, most of the blade's upper body and leading edge (colored lines) turn toward the suction side in this configuration, while the trailing edge and middle to lower half area of the blade remain in the undeformed reference shape. In Fig. 9, the morphing shape for a configuration aiming to maximize the turning angle is presented. Here, the leading and trailing edges of the blade move toward the pressure side almost all along the blade's radial length, while the mid chord sections displace toward the suction side. The modifications result in a higher camber for the overall blade's body. Lastly, in Fig. 10, a configuration aiming to maximize the metal angle only at the leading edge is presented. Here, most of the blade remains undeformed (dark blue area) and only the leading edge moves toward the suction side of the blade.

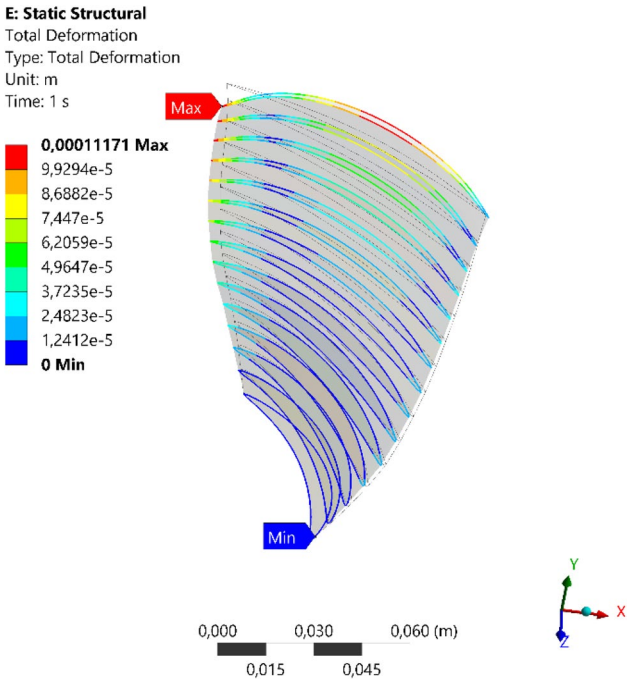

Fig. 9 Exemplary maximization of the turning angle for the NASA67 rotor blade

6 Aerodynamic analysis

Within the aerodynamic analysis, the resulting deformed shapes of the chosen test cases are compared to the original design blade geometry to evaluate the morphing potential for an aerodynamic performance improvement. For this, simplified actuation models with the same actuation behavior for contraction and expansion were implemented. The morphing

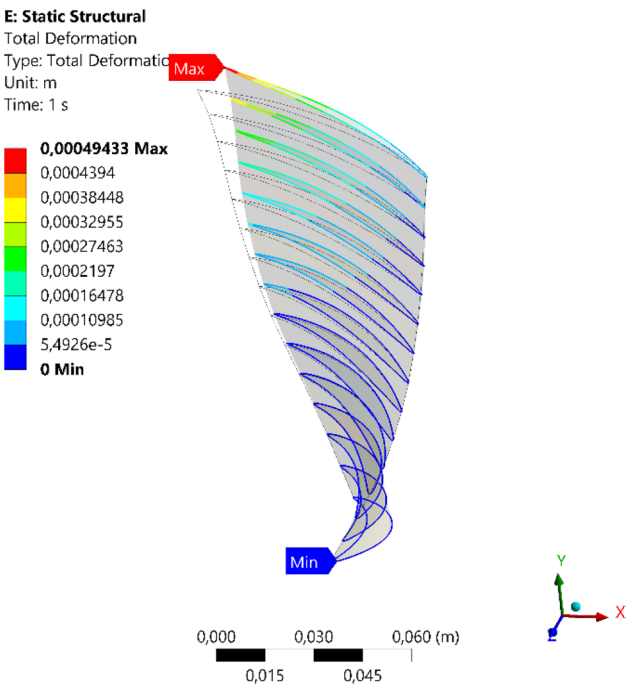

Fig. 8 Exemplary maximization of the metal angle for the NASA67 rotor blade

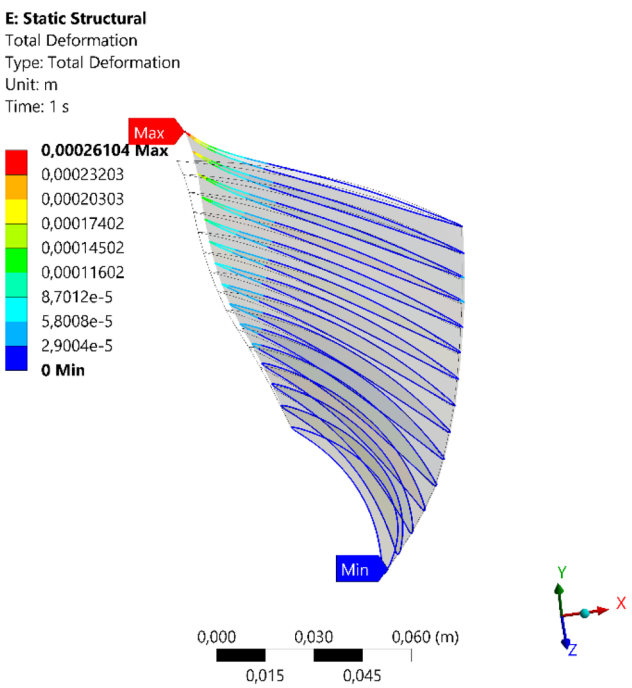

Fig. 10 Exemplary maximization of the metal angle at the leading edge for the NASA67 rotor blade

shapes from chapter 5.2 and future research consider the weaker compression behavior of the applied actuators. This reduces the achievable deformations for the contracted configuration.

6.1 Transfer from FEM to CFD

To evaluate the morphed rotor shapes, the discrete nodewise deformation data from the FEM simulation is transferred back into the aerodynamic pre-design space. Since the aerodynamic profile sections from the undeformed geometry are defined as a reference for the structural mesh, the mesh coordinates of the deformed geometry represent the deformed aerodynamic profile sections.

Contrarily to complex fluid structure interaction (FSI) problems in literature, which are for example based on moving mesh techniques or radial basis functions to overcome the discrepancies in mesh resolutions [25], this research aims for a coupling of the deformations data into the aerodynamic pre-design process. Next to simplified meridional flow calculations, the proposed methodology requires optimization routines. To efficiently evaluate different actuation concepts and blade reference shapes, rapid aerodynamic evaluation approaches are needed. Therefore, the re-engineering approach for compressor deterioration proposed by [18] is adapted, as it allows for a rapid evaluation of aerodynamic blade angle variations as well as for a precise re-engineering of the deformed rotor shapes, based on common meridional profile sections [19]. Due to the highly twisted and complex geometry of the transonic rotor blading, the creation of a structured mesh poses a major challenge, but allows to improve numerical efficiency and accuracy for the CFD simulations. The chosen re-engineering process therefore avoids moving mesh techniques and uses fully automated meshing routines for the morphed geometries that guarantee an adequate mesh quality. This is especially beneficial, since fillets are included for the rotor and stator geometries.

To evaluate the actuated rotor geometries according to aerodynamic design criteria, the grid point-based FEM output is re-engineered to match the geometry resolution required within the aerodynamic design. In Fig. 11, the FEA mesh resolution (red) is compared to the CFD resolution requirement (black), where the profile control points are barely distinguishable in the vicinity of leading and trailing edge. The sorting and the section-wise separation of the deformed rotor is conducted by comparing the point coordinates of the deformed blade to the meridional streamlines, which were used within the reference blade modeling. Before the profile sections are separated into their suction and pressure sides, the 3D representation of the profile sections is transformed back into a 2D conformal design representation. While the spanwise stagger angle variation $\Delta\lambda$ can be calculated through the shifted position of the leading and

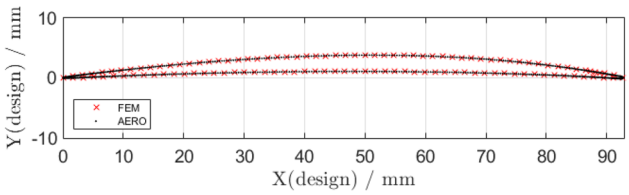

Fig. 11 Comparison of FEM resolution with the profile section resolution, required for CFD simulations

trailing edges, the estimation of the morphed profile turning $\Delta\Delta\varphi$ requires a re-engineering of the camber for each profile section. Thereby, the camber maximum and its chordwise position, as well as the camber angles at leading and trailing edge can be evaluated and compared to the respective values for the reference geometry.

Due to the lower mesh resolution of the structural mesh, especially in the leading and trailing edge areas, where a high geometric accuracy is required within the aerodynamic design, a CFD evaluation with the raw FEM output is not feasible. Under the assumption that the effects of the piezoceramic actuation are solely represented by variations in profile camber, while the thickness distribution of the profiles remains constant, the thickness distribution from the aerodynamic pre-design is superimposed onto the re-engineered camber, yielding a 2D representation of the deformed profile sections. Comparing the re-engineered profile sections again with the FEM point cloud shows that the uncertainties introduced by this assumption are negligible (see Fig. 11). By transforming the deformed profile sections back onto the cylindrical design-stream surfaces through the rotor, the re-engineering process is finalized and the individual profiles as well as the full blade can be evaluated through computational fluid dynamics (CFD) simulations. A detailed overview of the applied re-engineering process is described in Ref. [19].

6.2 Evaluation of the spanwise deformations

The evaluation of the spanwise turning and stagger variations induced by simplified models of the actuation concepts, introduced in chapter 5, indicates that the highest displacements are achieved toward the blade tip. Due to the chordwise clamping of the blade into the hub, the hub sections remain basically undeformed throughout the actuation. In Fig. 12, the spanwise morphing of the blade turning $\Delta\Delta\varphi$ and the leading edge metal angle morphing $\Delta\kappa_1$ are depicted depending on the radial position of the leading edge and the actuation target. Both blade design parameters define the ideal rotor inflow condition as well as flow turning capability and are therefore ideally suited for a preliminary aerodynamic morphing evaluation.

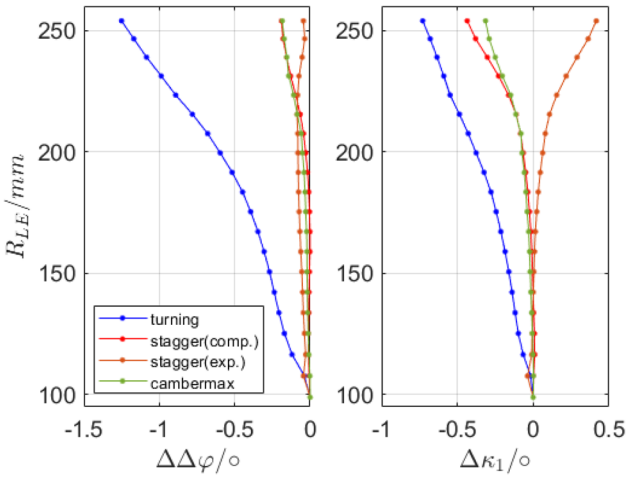

Fig. 12 Feasible variations in blade turning (left) and leading edge metal angle (right) deformation

Three exemplary actuation concepts are evaluated and named according to their dominant effect in the blade tip region:

1) Morphing of the blade turning (blue).
2) Increase (red) and decrease (orange) of the stagger angle.
3) Shift of the maximum camber position toward the trailing edge (green).

While the turning angle determines the achievable pressure ratio, the leading edge metal angle directly influences the design point inflow angle of the profiles. The turning angle variation is highest for cases such as the one depicted in Fig. 9, while the stagger angle adaption is negligible due to the symmetric nature of the introduced deformations.

A stronger adaption of the stagger angle is visible in cases such as the one in Fig. 8, which results in a maximum leading edge metal angle adaption of 0.34° at the blade tip, through expanding the actuators on the suction and pressure side. With the deformations dominating the leading edge area, also the blade turning is influenced, but less distinctly, compared to the turning adaption scenario.

By reversing the actuation mechanism of the suction side actuator in the twist adaption scenario, the stagger angle and therefore the leading edge metal angle adaption is also reversed, doubling the total amount of achievable deformation for a nearly constant actuator configuration (similar to the one in Fig. 10).

The smallest deformations in terms of blade turning and leading edge metal angle are achieved by trying to shift the maximum camber position rearward. However, instead an increased blade lean is realized toward the blade tip, through this actuation concept.

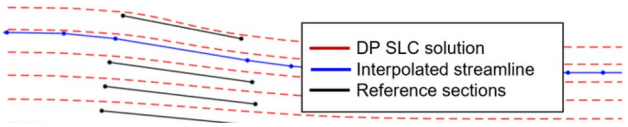

Fig. 13 Interpolation of the mean streamline based on blade reference sections and the design point (DP) SLC solution

6.3 Simplified aerodynamic Q3D evaluation

With the highest displacements toward the blade tip for all adaption scenarios, the transonic nature of the selected test case gains more importance, as the blade–shock interaction is rather sensitive to small changes in the profile geometry. This especially implies the suction side curvature beyond the leading edge toward a compression shock, which is typical for transonic compressor rotors. The comprehensive evaluation of the blade–shock interaction for the deformed geometries, however, is only feasible through CFD simulations.

Determining the optimal actuator configuration for a selected aerodynamic operation scenario (Fig. 4) requires optimization, which in combination with full 3D stage CFD simulations for the aerodynamic evaluation results in a high calculation effort, even for a single passage simulation. To avoid the increased computational effort, a representative quasi-three-dimensional (Q3D) simulation approach is introduced. As the achievable deformations are highest toward the blade tip, where the blade–shock interaction is highly sensitive toward small changes in geometry, a tip section at 95% rotor height is selected for the evaluation. Thereby, the direct influence of tip vortex and shroud end-wall boundary layer, which would occur in the tip region of a comparable 3D simulation is avoided. By evaluating the blade–shock interaction of the deformed rotor geometry, while considering the spanwise profile angle variations, introduced in Fig. 12, a preliminary decision on discarding or further investigating the actuation concept is possible.

Since the streamline positions alter depending on the mass flow and the pressure ratio of the selected adaption scenario (Fig. 4), the modeling of the CFD domain for the Q3D simulation approach is based on a streamline curvature calculation (SLC) for the reference design point and the reference blade section locations, defined in the meridional plane within the reference blade modeling. The reference blade sections are equally spaced over the blade height and serve as an input for the FEM simulations as well as the aerodynamic pre-design (Fig. 13).

The streamlines of the design point SLC solution are then interpolated onto the reference sections to model the mean line of the Q3D simulation domain. Thereby, the new streamline follows the linear slope of the profile section in the S2 plane. Beyond the blade row, the mean line is

interpolated between the neighboring reference streamlines of the DP SLC solution (Fig. 13).

To include 3D effects, such as end-wall boundary layers, compressibility and channel tapering, the axial velocity density ratio (AVDR) is considered in the simulation setup. The streamwise AVDR is calculated from the original SLC data presented in [22] and remodeled with a hyperbolic approach following the works of Stark [10]. In the hyperbolic approach, blade height and channel tapering length are adjusted until a suitable representation of the literature AVDR distribution is achieved (see Fig. 14).

With the hyperbolic AVDR distribution fitting the original AVDR from [22], a streamwise stream-tube height distribution is derived and applied orthogonally onto the mean interpolated streamline (Fig. 15, top). With a starting thickness of 1 mm at the domain inlet, the domain height is gradually reduced, following the increasing AVDR through the rotor blade row toward the domain outlet.

Through consideration of the AVDR within the simulation setup, the relative inflow angle is modified, affecting the blade–shock interaction and, through that, the achievable pressure ratio as well as the occurring profile losses (see Fig. 15). This again confirms the importance of including AVDR effects, especially for the investigation of transonic as well as supersonic profile sections, where the unique incidence condition dominates the profile performance [26].

For the final Q3D simulation domain, a cylindrical stream surface is derived and the deformed tip sections are projected onto the mean streamline to model the blade geometry within the CFD domain. A structured mesh is created in Numeca AutoGrid 5, with a y^+ of approximately 1 at the blade surface and two cells in radial direction. The upper and lower boundaries of the simulation domain are defined

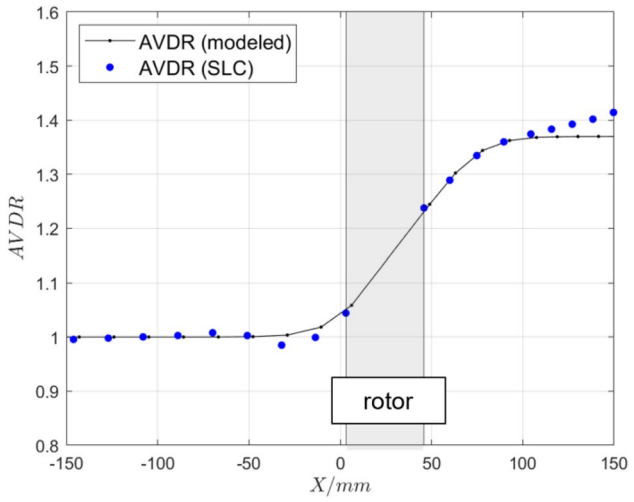

Fig. 14 Approximation of the streamwise AVDR distribution for the literature SLC solution [22]

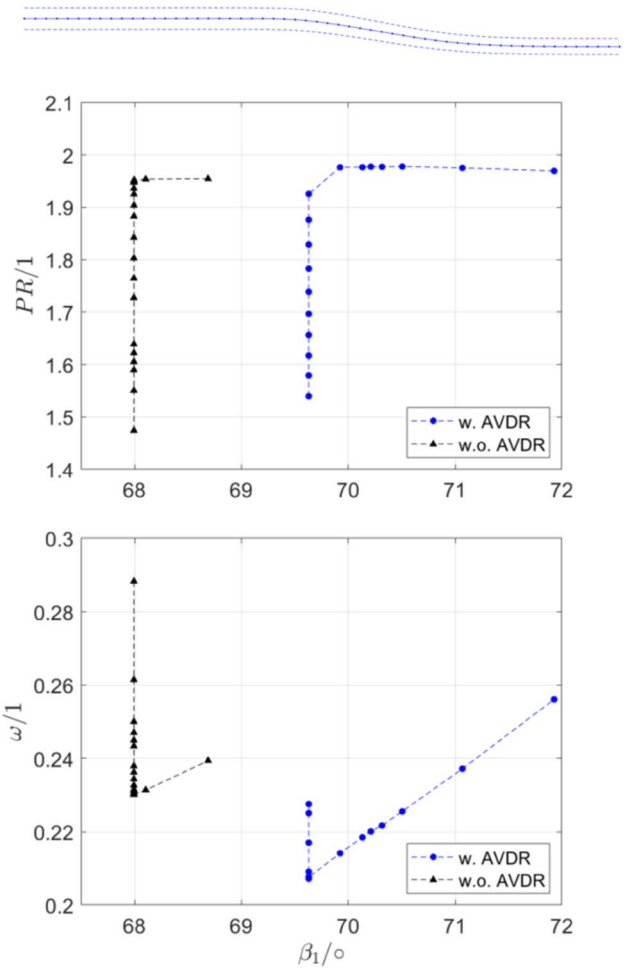

Fig. 15 Simulation domain in the meridional plane and impact of AVDR on the predicted performance

as no slip walls, while periodic boundary conditions are defined at the side panels of the domain to reduce the simulation domain to one blade passage. The speed lines of the deformed profiles are created by gradually increasing the static back pressure at the domain outlet. For the evaluation of the profiles, relative inflow angle, pressure ratio, flow turning as well as profile losses are considered.

Similarly, to the 3D stage model, a turbulence model study is conducted for the Q3D simulation setup, taking into account the calculation time, accuracy and the numerical stability. The main difference between the turbulence models is the numerical stability beyond the spill point, when the leading edge bow shock detaches from the profile. Here, the combination of an SST model with an additional transition model yields the highest stability toward increasing back pressures, while the pure SST model crashes immediately, when the back pressure exceeds the unique incidence condition (Fig. 16). According to literature, the suitability of the k-ε model near walls is limited, which only leaves the

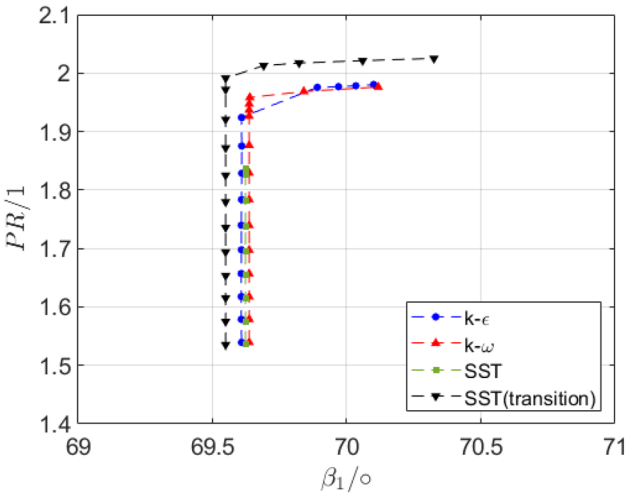

Fig. 16 Comparison of the speed lines of different turbulence models for the Q3D simulation setup

k-ω and the SST-transition model [27]. Although the combination of an SST approach with a transition model offers higher result accuracy, especially with the leading edge bow shock detached, the k-ω turbulence model is selected, mainly due to its numerical stability and speed. Additionally, the comparability between 3D and Q3D simulation results is ensured, by using the same turbulence model for the 3D and Q3D simulations (see Fig. 3).

The described CFD evaluation approach is applied to actuation concepts similar to those introduced in chapter 5. While the first actuation concept is expected to increase the achievable pressure ratio due to the increased blade turning, the morphing of the spanwise twist should affect the unique incidence condition toward the blade tip.

6.3.1 Adaption of maximum camber

An initial evaluation of the spanwise deformations yields an increase in blade turning through shape adaption of maximal 1.5° at the blade tip. However, as the relative inflow Mach number of 1.38 indicates the occurrence of strong shocks and a critical blade–shock interaction, the profile section performance is predicted differently through the CFD simulation. While a variation of the unique incidence angle is visible due to the variation of the leading edge metal angle and the suction side curvature, no increase in pressure ratio is achieved (Fig. 17).

With the increment of the maximum blade camber and a constant maximum camber position throughout the adaption, the suction side curvature toward the leading edge is increased, which leads to higher Mach numbers before the compression shock and thus to higher profile losses. The increased profile loss over the simulated operating range diminishes the benefits of the increased blade

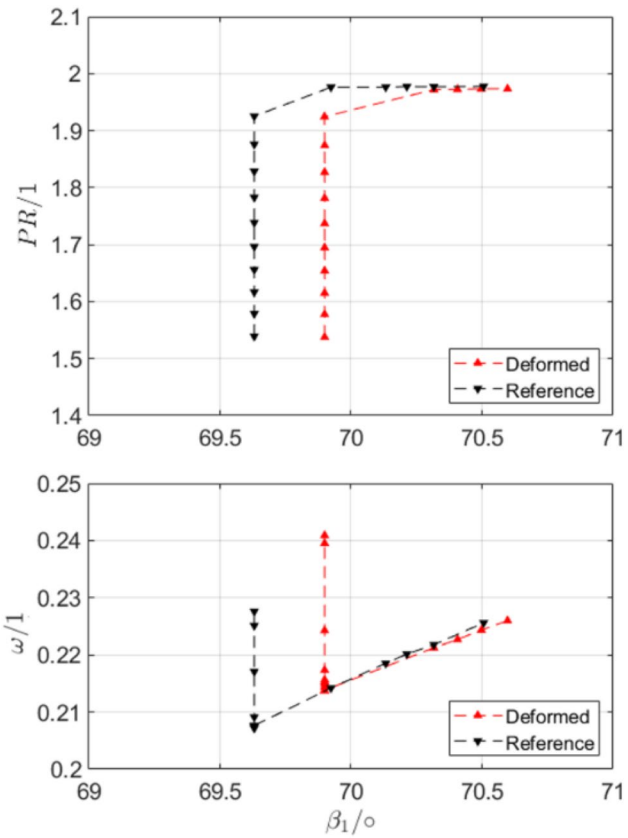

Fig. 17 Achievable pressure ratio (top) and profile losses (bottom) due to camber morphing/comparison with reference profile section

turning, mainly due to the adverse effects of the blade–shock interaction.

6.3.2 Adaption of blade twist

By changing fiber orientation and actuator placement, the morphing of the blade sections can modify the blade twist as shown in Figs. 8 and 10. Again, this deformation is increasingly noticeable toward the blade tip, while the hub sections remain undeformed throughout the adaption.

By switching the actuation mechanism from expansion to compression for the present actuator placement, the shape morphing can be reversed, provided an equally strong compression and expansion behavior of the actuators is assumed. The achievable deformations are concentrated in the tip region of the profile section, increasing the unique incidence angle for compression or reducing it for expansion (Fig. 18). Compressing the actuators increases suction side curvature, causing a slight increase in shock loss and a reduction of the achievable pressure ratio. The Q3D simulations, however, confirm the expected effect of an increasing twist variation toward the blade tip on the performance of a transonic rotor section. While the analysis of the structural simulation data

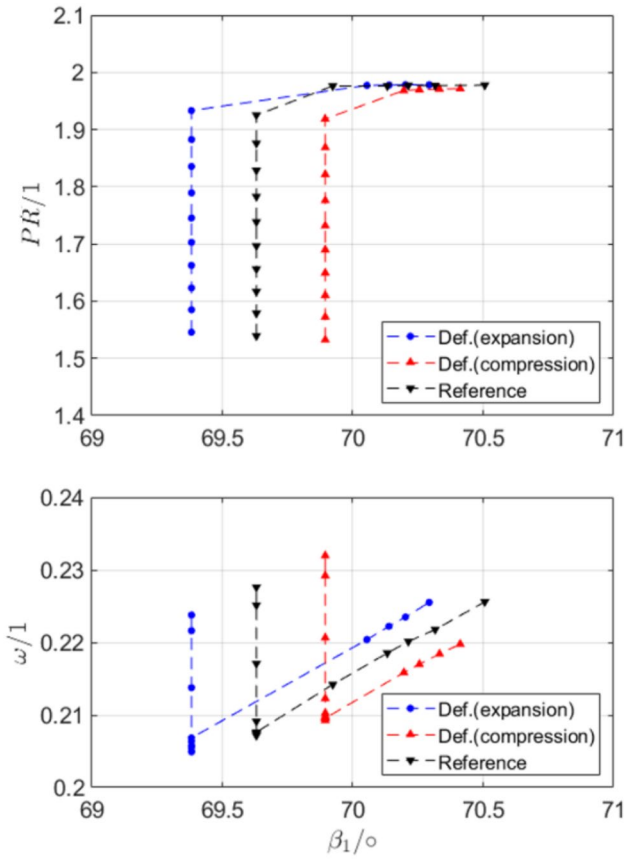

Fig. 18 Achievable pressure ratio (top) and profile loss variation (bottom) due to morphing the spanwise twist/comparison with reference profile section

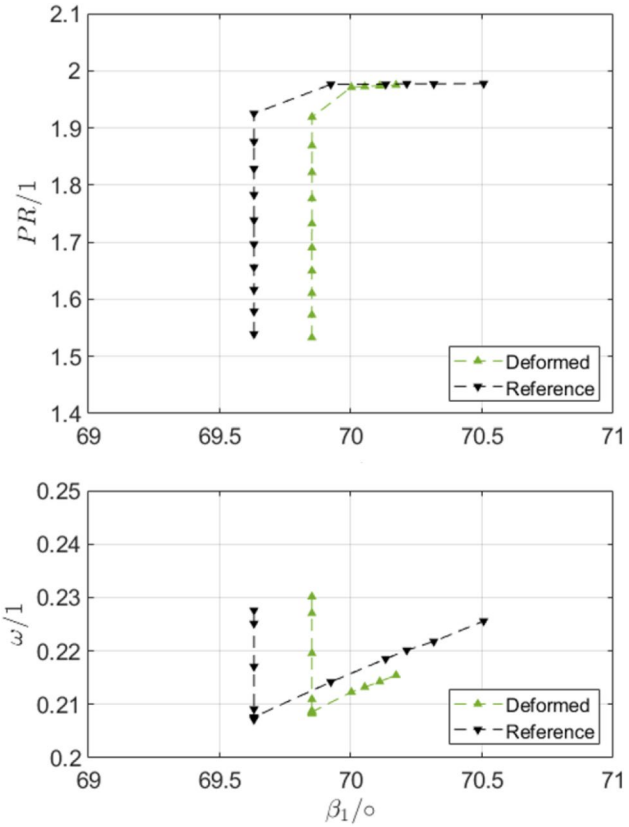

Fig. 19 Achievable pressure ratio (top) and loss variation (bottom) due to an attempted rearward shift of the blade maximum camber/comparison with reference profile section

yields a total leading edge metal angle variation of 0.48° at 95% blade height, the CFD simulation predicts a 0.51° variation of the unique incidence angle between expanded and compressed actuator condition.

6.3.3 Adaption of maximum camber position

As shown in Ref. [28], the deformation of transonic rotor tip sections toward a rearward shift of the maximum camber is especially beneficial for increasing the achievable pressure ratio while reducing the profile losses for a selected off-design adaption scenario. Although this deformation requirement poses a challenge for the piezoceramic actuation, a slight shift of the maximum camber position toward the blade trailing edge is feasible with the third actuation configuration. However, the rearward camber shift is superimposed with a stagger angle variation and a structurally increased blade lean of the tip sections.

The feasible rearward shift of the maximum camber position appears to be too small to show the expected impact on the blade profile performance. Due to the adaption of the blade leading edge metal angle, the shift of the unique incidence condition toward higher inflow angles is dominant, while minimum profile loss and achievable pressure ratio remain constant (Fig. 19). Comparing these results to the adaption of the blade twist in the previous chapter, the achievable shift of the unique incidence angle with 0.23° is rather small. More interesting for this actuation configuration could be the achievable increase in blade lean. This however indicates a limit of the proposed Q3D evaluation approach, as 3D effects, evoked by lean and sweep cannot be captured by a representative profile section simulation, but merely require a full 3D simulative approach.

6.4 Evaluation of 3D stage aerodynamics

To verify the conclusions drawn from the deformation evaluation and the Q3D simulation approach, the deformed blade of the turning adaption configuration (Fig. 9) is fully re-engineered and prepared for a 3D CFD evaluation with the stage setup described in chapter 4. Special emphasis thereby lies on the 3D effect of the increased suction side curvature, which has already been indicated as a crucial design parameter within the representative Q3D approach.

By increasing the leading edge metal angle through the higher blade cambering, the choke mass flow is decreased, compared to the performance of the reference design (Fig. 20). As already indicated by the Q3D simulation, the reduced throat area and therefore a shift in the unique incidence angle can be identified as the major cause for the mass flow variation toward the choke limit. With increasing back pressure, the speed line of the morphed rotor converges back toward the speed line of the reference design, until simulation divergence indicates the numerical onset of stall, which in this case corresponds to the operating point, where the leading edge bow shock detaches from the blade in the sonic regimes of the rotor.

The predicted stage efficiency remains below the reference design's efficiency over the simulated operating range, which is mainly driven by the increased Mach numbers toward the compression shock in the upper area of the morphed rotor. With the back pressure rising, the passage shock position moves toward the leading edge, with an increasing part of the blade passage contributing to the flow deflection behind the compression shock. Therefore, the achievable pressure ratio is lifted slightly above the reference design, although the stage efficiency remains lower (Fig. 20, bottom).

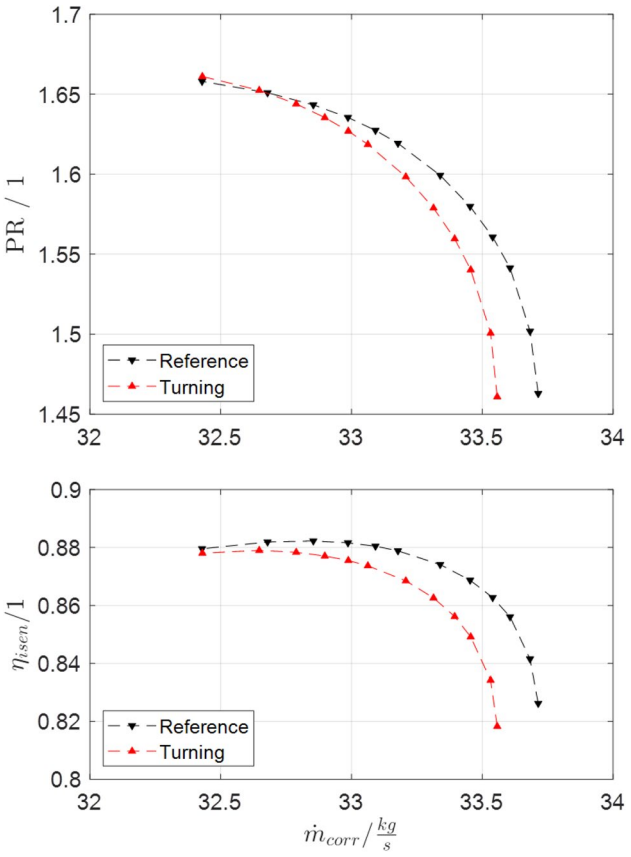

Fig. 20 Speed line (top) and efficiency variation (bottom) for the 3D morphed rotor (turning adaption) compared to the reference blade design

6.5 Conclusion on the evaluation methodology

The comparison of the 3D-CFD results with the aerodynamic blade angle variations displayed in (Figs. 8 and 10) shows that the transformation of the simulated displacements into aerodynamic blade design criteria is already a good indicator for the full 3D stage performance. However, for transonic and supersonic inflow conditions, the exclusive interpretation of the turning variation is no reliable indicator for the achievable increase or decrease of the pressure ratio, as the suction side curvature plays a decisive role in the performance of the chosen test case. This over-simplification is evaded, through the introduction of the representative Q3D simulation approach, which already allows similar conclusions as the full 3D CFD simulation, such as the choke mass flow variation due to the unique incidence condition or the influence of the blade–shock interaction on the stage performance.

7 Conclusions and outlook

This study presents an aerodynamic evaluation methodology for the potential of structural morphing applied to compressor blades. The NASA67 rotor was chosen as a case scenario.

For the structural modeling and analysis of the morphing blade, a standard homogeneous titanium alloy blade structure was defined. MFC piezo actuators were embedded onto the blade's structure, allowing the introduction of the morphing behavior. Three different possible morphing configurations were analyzed: a modification of the twist angle, an increment in the amplitude of the blade's maximum camber and a displacement of the maximum camber from its position at the center of the blade toward the trailing edge. These deformations were the result of different actuator configurations for the blade, meaning the number of actuators, their sizes, positions and the actuation directions could be modified.

The resulting morphed shapes were then analyzed based on aerodynamic profile design criteria and the introduction of a representative Q3D analysis for a detailed aerodynamic performance evaluation. The analysis showed that the different actuator configurations do lead to changes in the flow characteristics and therefore to the blade's performance. For each of the chosen configurations, representative gain and loss values were calculated for a representative tip section at 95% blade height. This section was chosen as representative for its higher deformations and the sensitivity of the

supersonic flow toward small changes in blade profile geometry. Additionally, the influence of AVDR and the turbulence modeling approach within the aerodynamic evaluation simulation were included. A full 3D stage simulation of the turning adaption scenario showed that the simplified Q3D evaluation approach already gives a comprehensive picture of what aerodynamic behavior to expect from the morphed rotor blade. This especially includes the suction side curvature, which is neglected within the mere interpretation of the spanwise blade angle variation.

From a structural point of view, following studies will expand and analyze the potential of non-homogeneous materials for the blade, such as the use of fiber-reinforced composites. The analysis will also expand to include rotational and aerodynamic loads and to perform hot–cold shape transformations. This will serve to demonstrate the actuators' performance under operational conditions and to calculate the cold, manufacturable shapes of the morphing blade. Finally, both disciplines will be brought together to produce blade designs that selectively take advantage of the geometric changes and use them to reach more gains in performance while reducing losses, so that optimal efficiency values at design and off-design conditions can be achieved.

Acknowledgements We would like to acknowledge the funding by the Deutsche Forschungsgemeinschaft (DFG, German Research Foundation) under Germany's Excellence Strategy—EXC 2163/1- Sustainable and Energy Efficient Aviation–Project-ID 390881007.

Author contributions All authors contributed to the conception of this work as well as to the presented method's development. The manuscript was written by ZMR, with a special focus on Sects. 1–5 and 7; and MS, with a special focus on Sects. 1–4, 6 and 7. The contents were reviewed and feedback was given by JR and JF, who also supervised the work. All authors read and approved the final manuscript.

Funding Open Access funding enabled and organized by Projekt DEAL.

Declarations

Conflict of interest The authors have no known competing interests to declare that are relevant to the content of this article.

References

1. Monner, H.P., Huxdorf, O.: Design and manufacturing of morphing fan blades for experimental investigations in a cascaded wind tunnel. AIAA Sci .Tech. **2019**, 1 (2019)
2. Hünecke, K.: Jet engines: Fundamentals of theory, design and operation. Airlife, Shrewsbury (1997) [The Crowood Press, 1st edn. ISBN-10 : 9781853108341, ISBN-13 : 978-1853108341 (2010)]
3. Okura, T.: Materials for Aircraft Engines; Aircraft Propulsion ASEN 5063. https://www.colorado.edu/faculty/kantha/sites/default/files/attached-files/73549-116619_-_takehiro_okura_-_dec_17_2015_1027_am_-_asen_5063_2015_final_report_okura.pdf (2015). Accessed 10 Dec 2021
4. Storm, R., Skor, M., Koch, L.D., Benson, T., Galica, C.: Pushing the Envelope: A NASA Guide to Engines; NASA Glenn Research Center Office of Educational Programs in Cleveland: Celveleand. OH, USA (2007)
5. GE Fans Out on Testing of New GE9X Fan Blades: New Material and Design Improvements Drive High Aero-dynamic Performance. https://www.geaviation.com/press-release/ge90-engine-family/ge-fans-out-testing-new-ge9x-fan-blades. Accessed 8 Dec 2021
6. Rolls-Royce Starts Manufacture of World's Largest Fan Blades—Made of Composite Material—For Next-Generation UltraFan®Demonstrator. https://www.rolls-royce.com/media/press-releases/2020/11-02-2020-intelligentenginerr-starts-manufacture-of-world-largest-fan-blades.aspx. Accessed 10 Dec 2021
7. Aungier, R.H.: Axial-flow compressors. A strategy for aerodynamic design and analysis. American Society of Mechanical Engineers, New York NY USA (2003)
8. Joos, F.: Aerodynamik Axialer Turbokompressoren, 1st edn. Springer Vieweg, Wiesbaden, Germany (2020)
9. Bross, S., Stark, U.: Entwicklung neuer Schaufelgitter aus Profilen variabler Geometrie zum Einsatz in Leiträdern drallgeregelter Turbomaschinen—Teil II. Forsch. Im Ing. **60**, 120–132 (1994)
10. Stark, U.: Ebene Verdichtergitter in Quasizwei-dimensionaler Unterschallströmung, pp. 1–64. VDI-Forschungs-heft/Verein Deutscher Ingenieure (641/87), Düsseldorf, Germany (1987)
11. Mazzawy, R. S.; Virkler, J.: Variable pitch fan - the solution to achieving high propulsive efficiency turbofan engines. In: sae technical paper series. Aerospace technology conference and exposition, NOV. 10, 2009: SAE International400 Commonwealth Drive, Warrendale, P), United States (SAE Technical Paper Series). (2009)
12. Denning, RM.: (03261972): Variable Pitch Ducted Fans for STOL Transport Aircraft. In: ASME 1972 International Gas Turbine and Fluids Engineering Conference and Products Show. ASME 1972 International Gas Turbine and Fluids Engineering Conference and Products Show. San Francisco, California, USA, 26.03.1972 - 30.03.1972: American Society of Mechanical Engineers
13. Siemann, J., Krenz, I., Seume, J.R.: Experimental investigation of aspiration in a multi-stage high-speed axial-compressor. In: Proceedings of the ASME Turbo Expo: Turbine Technical Conference and Exposition – 2016, Seoul, South Korea; International Gas Turbine Institute; GT. New York, N.Y.: The American Society of Mechanical Engineers. (2016)
14. Montano, Z., Seidler, M., Riemenschneider, J., Friedrichs, J.: A coupling method for the design of shape-adaptive compressor blades. Appl Mech **3**(1), 182–209 (2022). https://doi.org/10.3390/applmech3010014

15. Woods, B. K.; Friswell, M. I.: Fluid-Structure Interaction Analysis of the Fish Bone Active Camber Mechanism. In: 54th AIAA/ASME/ASCE/AHS/ASC Structures, Structural Dynamics, and Materials Conference. Boston, Massachusetts. Reston, Virginia: AIAA. (2013)
16. Krawczyk, P., Beyene, A., MacPhee, D.: Fluid structure interaction of a morphed wind turbine blade. Int. J. Energy Res. **37**(14), 1784–1793 (2013). https://doi.org/10.1002/er.2991
17. Kamakoti, R., Shyy, W.: Fluid–structure interaction for aeroelastic applications. Prog Aerosp Sci **40**(8), 535–558 (2004). https://doi.org/10.1016/j.paerosci.2005.01.001
18. Reitz, G.; Friedrichs, J.: Procedure for analyzing, manipulating and meshing of compressor blades to simulate their flow. Int. J. Gas Turbine, Propuls Power Syst **8**. (2016)
19. Seidler, M.; Montano, Z.; Friedrichs, J.; Riemenschneider, J.: Introduction and evaluation of an aerostructural coupling approach for the design of shape adaptive compressor blading. In. Proceedings of the 25th ISABE Conference, Ottawa. Ontario, Canada. (2022) (in press)
20. SMART MATERIAL, "MFC Overview," URL: https://www.smart-material.com/MFC-product-mainV2.html. Accessed 4 Aug 2021
21. CompActive, "Product catalogue for standard configurations and samples," URL: https://compactive.de/products/. Accessed 4 Aug 2021
22. Strazisar, A.J., Wood, J.R., Hathaway, M.D., Suder, K.L.: Laser anemometer measurements in a transonic axial-flow fan rotor. NASA Technical Paper **2879**, 1 (1989)
23. Reis, A.: Validation of NASA Rotor 67 with OpenFOAM's Transonic Density-Based Solver, Faculdade de Ciências e Tecnologia – Universidade Nova de Lisboa. (2013)
24. Friendship Systems, "CAESES®: Solutions for Turbomachinery Design," URL: https://www.friendship-systems.com/solutions/for-turbomachinery/. Accessed 7 Jan 2021
25. Groth, C., Porziani, S., Biancolini, M.E.: Radial basis functions vector fields interpolation for complex fluid structure interaction problems. Fluids **6**(9), 314 (2021). https://doi.org/10.3390/fluids6090314
26. Cumpsty, N.A.: "Compressor aerodynamics", reprint edition 2004 w/new preface, introduction and updated bibliography. Krieger Publishing Company, Malabar, Florida (2004)
27. Laurien, E., Oertel, H.: Numerische Strömungs-mechanik. Springer Fachmedien Wiesbaden, Wiesbaden (2018)
28. Seidler, M., Friedrichs, J. et al.: Introduction of an improved axial compressor profile shape modelling approach for increased flexibility in transonic profile design", Proceedings of Global Power and Propulsion Society (in press.) (2021)